Supporting information

Phase and Interface Engineering of a Ru-Sn Nanocatalyst for Enhanced Alkaline Hydrogen Oxidation Reaction

Licheng Wei[†a], Wei Yan[†a], Zhongliang Huang[a], Ruchun Li[d], Qingyu Kong[e], Wei-Hsiang Huang[f], Chih-Wen Pao[f], Zhiwei Hu[g], Haixin Lin[a,h], Nanjun Chen[a], Yong Xu[c*], Hongbo Geng[b*], and Xiaoqing Huang[a,h*]

[a]State Key Laboratory of Physical Chemistry of Solid Surfaces, College of Chemistry and Chemical Engineering, Xiamen University, Xiamen, 361005, China.
[b]School of Materials Engineering, Changshu Institute of Technology, Changshu, 215500, China.
[c]i-lab, Suzhou Institute of Nano-Tech and Nano-Bionics (SINANO), Chinese Academy of Sciences (CAS), 398 Ruoshui Road, Suzhou, 215123, China.
[d]Faculty of Chemistry and Chemical Engineering, Yunnan Normal University, Kunming, 650500, Yunnan, China.
[e]Synchrotron Soleil, L'Orme des Merisiers, St-Aubin, Gif-sur-Yvette 91192 CEDEX, France.
[f]National Synchrotron Radiation Research Center, 101 Hsin-Ann Road, Hsinchu 30076, Taiwan.
[g]Max Planck Institute for Chemical Physics of Solids Nothnitzer Strasse 40, Dresden 01187, Germany.
[h]Innovation Laboratory for Sciences and Technologies of Energy Materials of Fujian Province (IKKEM), Xiamen University, Xiamen, 361005, China.

[*]E-mail: yxu2023@sinano.ac.cn; hbgeng@cslg.edu.cn; hxq006@xmu.edu.cn

METHODS

Chemicals. Ruthenium (III) chloride hydrate ($RuCl_3 \cdot xH_2O$, 99.98%) was obtained from Sigma-Aldrich. Tin(II) acetate ($Sn(CH_3COO)_2$, 98%) was purchased from Zhengzhou Speak Chemical Co. Ltd. Oleylamine ($C_{18}H_{37}N$, 70%) was purchased from J&K Scientific Ltd. Potassium hydroxide (KOH), isopropanol (C_3H_8O, AR), and ethanol (C_2H_6O, AR) were purchased from Sinopharm Chemical Reagent Co. Ltd. (Shanghai, China). Commercial Pt/C (20 wt.%) was obtained from Johnson Matthey (JM). Water (18 MΩ cm^{-1}) used in all the experiments was obtained by passing through an ultrapure purification system (Aqua Solutions). All the chemicals were used as received without further purification.

Materials synthesis. For $fcc_{0.42}$ Ru-Sn, $RuCl_3 \cdot xH_2O$ (10 mg), $Sn(CH_3COO)_2$ (1.5 mg), and 5 mL oleylamine were added into a glass vial (volume: 30 mL). After capping the vial, the mixture was ultrasonicated for 1 h, which was subsequently heated to 235 °C and maintained at the same temperature for 5 h in oil bath. After cooling to room temperature, the black products were collected and washed with an ethanol/cyclohexane three times by centrifugation. The synthesis of fcc_x Ru-Sn was similar to that of $fcc_{0.42}$ Ru-Sn excepting for changing the amount of $Sn(CH_3COO)_2$ (0, 0.7, 3, and 11.2 mg) for hcp Ru, $fcc_{0.25}$ Ru-Sn, $fcc_{0.63}$ Ru-Sn, and fcc Ru-Sn, respectively.

Characterizations. Transmission electron microscopy (TEM) was operated on JEOL electron microscope at an accelerating voltage of 100 kV. High-resolution TEM (HRTEM) and energy dispersive X-ray spectroscopy elemental mapping were operated on FEI Tecnai F30 TEM with an accelerating voltage of 300 kV. Energy dispersive spectrometer (EDS) was conducted on Sigma with an accelerating voltage of 15 kV. X-ray diffraction spectroscopy (XRD) was conducted on Rigaku with Cu Kα (λ = 1.54 Å). X-ray photoelectron spectrum (XPS) was conducted on SSI S-Probe XPS spectrometer. Thermogravimetric (TG) curves were obtained through a STA209 PC (Netzsch, Germany) instrument from 25 to 900 °C. The H_2 temperature programmed desorption (H_2-TPD) was conducted with the Micro. AutoChem II 2920, 50 mg of the sample was preprocessed in Ar environment at 300 °C for 2 h, and then cooled down to 30 °C for adsorbing hydrogen for 1 h in 5% H_2/Ar combination gas, finally increased temperature to 700 °C under Ar environment to collect signal. XAS was operated on NSRRC TPS44A and Soleil Synchrotron (France), ODE beamline.

Rietveld Refinement for fcc_x Ru-Sn. X-ray diffraction (XRD) pattern was indexed as fcc Ru and hcp Ru using Jade. Hereafter, the Rietveld refinement was performed on TOPAS program according to initial model of fcc Ru (PDF: 88-2333) and hcp Ru (PDF: 88-1734). The background, scale factor, zero, cell parameters, and profile parameters, such as U, V, and W of Pseudo-Voigt function, were refined. Herein, we fixed all the atom coordination. And the final reliable factors of samples listed in Table S1.

Electrochemical measurements. All the electrochemical measurements were performed at CHI660 electro-chemical workstation (Chenhua, shanghai) with a typical three-electrode system. A rotating disk electrode (RDE) with diameter of 5 mm, graphite rod, and a saturated calomel electrode (SCE) were used as working electrode, counter electrode and reference electrode, respectively. For the preparation of the working electrode, catalysts were loaded on carbon black (Vulcan XC-72R) by ultrasound 1 h. The loading content of Ru on carbon powder was estimated from TG analysis and EDS composition. The catalyst (1 mg), isopropanol (495 μL), and Nafion solution (5 μL, 5 wt.%) were added into a glass vial and then ultrasonicated for 1 h to make a homogenous ink. Then, electrocatalyst ink was dropped onto the RDE surface. The loading content of electrocatalyst was 2.5 μg on the RDE. All electrochemical

performance of catalysts was tested after activating for 20 cycles at a scan rate of 0.5 V s^{-1} during potential range from −0.2 to 0.4 V vs. RHE. Linear sweep voltammetry (LSV) was carried out at the scan rate of 5 mV s^{-1} and rotation speed of 1600 rpm. All the polarization curves were corrected 95% IR compensation by workstation. The kinetic current density (j_k) can be calculated by the Koutecky-Levich (K-L) equation (1):

$$1/j = 1/j_k + 1/j_d \quad (1)$$

where j and j_d represent as the current and the diffusion-limited current, respectively. j_d can be collected by the Levich equation (2):

$$j_d = 0.62nFD^{3/2}v^{-1/6}C_0\omega^{1/2} = BC_0\omega^{1/2} \quad (2)$$

where n is the number of electrons involved in the HOR, F is the Faraday constant, D is the diffusion coefficient of the reactant, v is the viscosity coefficient of electrolyte, C_0 is the solubility of H_2 in the electrolyte, ω is the rotating speed, and B is the Levich constant.

The exchange current density j_0 can be obtained from the Butler-Volmer (B-V) equation (3):

$$j_k = j_0(e^{\alpha F/RT} - e^{(-\alpha)F\eta/RT}) \quad (3)$$

where α is the transfer coefficient, F is the Faraday constant, R is the universal gas constant, T is the temperature, and η is the overpotential.

Electrochemically surface areas (ECSAs) were tested by Cu underpotential deposition (Cu_{UPD}) stripping experiment. Typically, CV on each catalyst was first carried out at a scan rate of 50 mV s^{-1} in Ar-purged 0.5 M H_2SO_4 solution to obtain a steady voltammogram as the background. Then, Cu_{UPD} stripping was performed at a scan rate of 50 mV s^{-1} in Ar-purged 0.5 M H_2SO_4 solution after Cu deposition in Ar-purged 0.5 M H_2SO_4 solution containing 5 mM $CuSO_4$ at about 0.24 V for 100 s. The value of ECSA (cm^2) can be calculated by equation (4):

$$ECSA = Q_{Cu}/Q_s \quad (4)$$

where Q_{Cu} is the measured integral charge, Q_s is the surface charge density of 420 μC cm_{metal}^{-2} which is assumed for a monolayer adsorption of Cu_{UPD} on metal.

Accelerated durability test (ADT) was operated by CV cycles in H_2 or H_2 + 1000 ppm CO-saturated 0.1 M KOH electrolyte.

CO stripping test was performed in 0.1 M KOH solution. First, the electrode was held at a certain potential for 100 s in CO-saturated 0.1 M KOH solution to adsorb CO. Then, the electrode was rapidly transferred to the Ar-saturated 0.1 M KOH solution, and CV curves were collected in the potential range from 0 to 1 V vs. RHE at a scan rate of 50 mV s^{-1}. The obtained first forward scan is considered as the stripping of a monolayer of CO.

MEA tests. $fcc_{0.42}$ Ru-Sn /C with a loading amount of 0.08 mg_{Ru} cm^{-2} and Pt/C (40 wt.% Pt, Johnson Matthey) with a loading amount of 0.2 mg_{Pt} cm^{-2} were used as the anode and cathode catalyst, respectively. For comparison, Pt/C (40 wt.% Pt, Johnson Matthey) or PtRu/C (40 wt.% Pt and 20wt.% Ru, Johnson Matthey) with a loading amount of 0.08 mg_{Pt} cm^{-2} or 0.08 mg_{Pt+Ru} $cm^{-2}$and Pt/C (40 wt.% Pt, Johnson Matthey) with a loading amount of 0.2 mg_{Pt} cm^{-2} were used as the anode and cathode catalyst,

respectively. The hydroxide exchange membrane and ionomer were synthesized as reported before.[1] The catalyst ink was prepared by ultrasonically dispersing the catalysts and ionomer into water and isopropanol (1:10 v/v) for 1 h. The ratio of catalysts to ionomers is 4:1. Afterwards, the catalyst ink was sprayed onto both sides of home-made poly(aryl-co-aryl piperidinium) anion exchange membrane (28 μm) to fabricate a catalyst coated membrane (CCM) with the electrode area of 5 cm^2. All CCMs were immersed into 1 M KOH solution for overnight for performance test and then rinsed thoroughly with deionized water to remove all excess KOH. CCMs in the wet state were directly assembled with two gas diffusion layers (GDLs), fluorinated ethylene propylene (FEP) gaskets, and graphite bipolar plates with a 5 cm^2 flow field to obtain a complete AEMFC using a torque of 5 N. The actual catalyst loading of MEAs was slightly adjusted by the area swelling of wet CCMs. AEMFC performance was measured using a fuel cell test station (850E Multi Range). The flow rates of H_2/100 ppm CO/H_2 and O_2/Air (CO_2-free) gases were set as 1.0 L min^{-1} with 200 kPa of backpressures. The anode and cathode of the humidifying temperature were set at 92 and 94 °C, respectively. The cell temperature was set at 97 °C. Stability test conditions are listed as follow: cell temperature at 80 °C, anode humidifier temperature at 79 °C and cathode humidifier temperature at 80 °C, back pressures were symmetric at 100 kPa, H_2 flow rate at 0.3 L min^{-1} and O_2 flow rate at 0.3 L min^{-1}.

Electrochemical measurement of *in-situ* Fourier transform infrared spectroscopy (FTIR). Electrochemical *in-situ* Fourier transform infrared spectroscopy experiments were carried out on a Nicolet 8700 FTIR spectrometer equipped with a liquid-nitrogen-cooled MCT-A detector. A thin-layer IR cell with a CaF_2 prism was used. During the external reflection FTIR measurement, a thin layer structure (~10 μm) is formed between the electrode and the IR window, and the signal is acquired during the process using a multi-step FTIR spectroscopy (MSFTIR) program. In the attenuated total reflection (ATR) FTIR experiment, the catalyst was directly dropped on the Si prism coated with Au film as the working electrode. The resulting spectra were reported as the relative change in reflectivity at each potential, that is, $\Delta R/R = R(E_S) - R(E_R) / R(E_R)$, where $R(E_S)$ and $R(E_R)$ are single-beam spectrum collected at the sample potential E_S and reference potential E_R, respectively. The E_S was switched from lower to higher potentials during the measurements. To improve the signal to noise ratio, 200 single-beam spectra were collected and co-added for each resulting spectrum at a spectral resolution of 8 cm^{-1}.

Ab initio calculation details. The slab models of the (111) plane of cubic Ru (space group: Fm-3m) and the (001) plane of the hexagonal Ru (space group: P63/mmc) phase were constructed and orthogonalized. The lattice mismatch between the two resulting surfaces is less than 2 %. The Sn-substituted in-plane heterojunction was built by replacing one of the surface Ru atoms belonging to the cubic phase with a Sn atom. The bare models along with H^-, OH^-, H_2O^-, CO^-, and $COOH^-$ adsorbed ones containing vacuum layers of at least 15 Å, were optimized based on the density functional theory (DFT) implemented in the Vienna Ab initio Simulation Package (VASP).[2] The ionic positions of those surface models were relaxed, whereas volumes and shapes of the unit cells were fixed. We employed the projector-augmented wave (PAW) pseudopotentials[3] to account for the ion cores and the Perdew-Burke-Ernzerhof (PBE) functional of generalized gradient approximation (GGA)[4] to calculate the exchange-correlation interactions of valence electrons. The weak dispersion interactions were corrected with Grimme's D3 scheme.[5] The plane waves were expanded using a cutoff energy of 400 eV and the Brillouin zone (BZ) was integrated with a Γ-centered Monkhorst-Pack 3 x 3 x 1 k-point grid. The Hellmann-Feynman forces acted on each atom and total energy between each electronic iteration were con-verged to 0.03 eV/Å and 1 x 10^{-6} eV,

respectively. We carried out vibration frequency calculations and derived thermal correction terms to the Gibbs free energies of adsorbates with the aid of the VASPKIT[6] code.

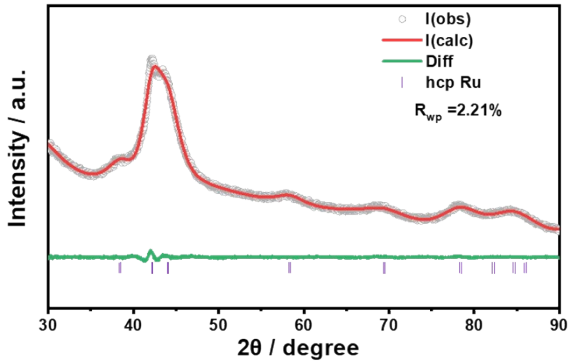

Fig. S1. Rietveld refinement of hcp Ru. The black circle curve and red curve represent as the measured and the fitting pattern, respectively, while the bottom line (green) is the difference profile.

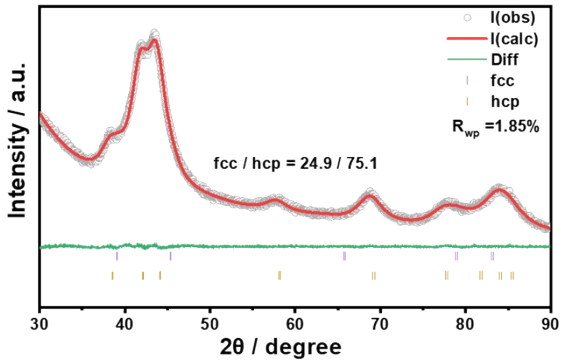

Fig. S2 Rietveld refinement of $fcc_{0.25}$ Ru-Sn. The black circle curve and red curve represent as the measured and the fitting pattern, respectively, while the bottom line (green) is the difference profile.

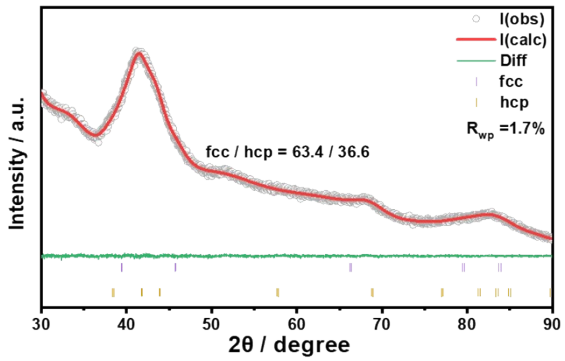

Fig. S3 Rietveld refinement of $fcc_{0.63}$ Ru-Sn. The black circle curve and red curve represent as the measured and the fitting pattern, respectively, while the bottom line (green) is the difference profile.

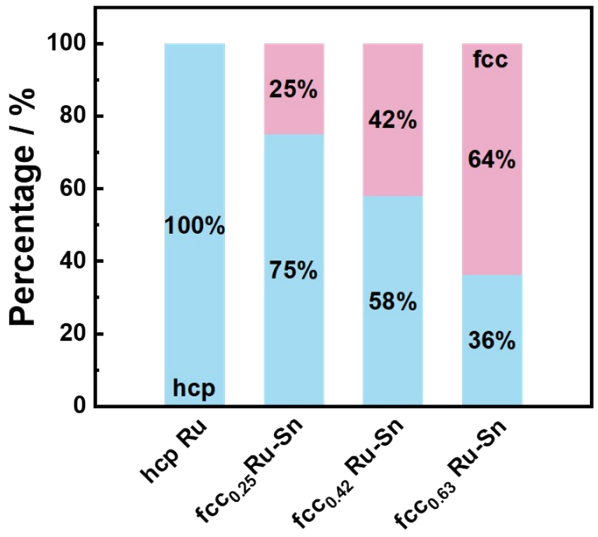

Fig. S4 The proportion change of two phases in samples (blue and pink represent as hcp and fcc phase, respectively).

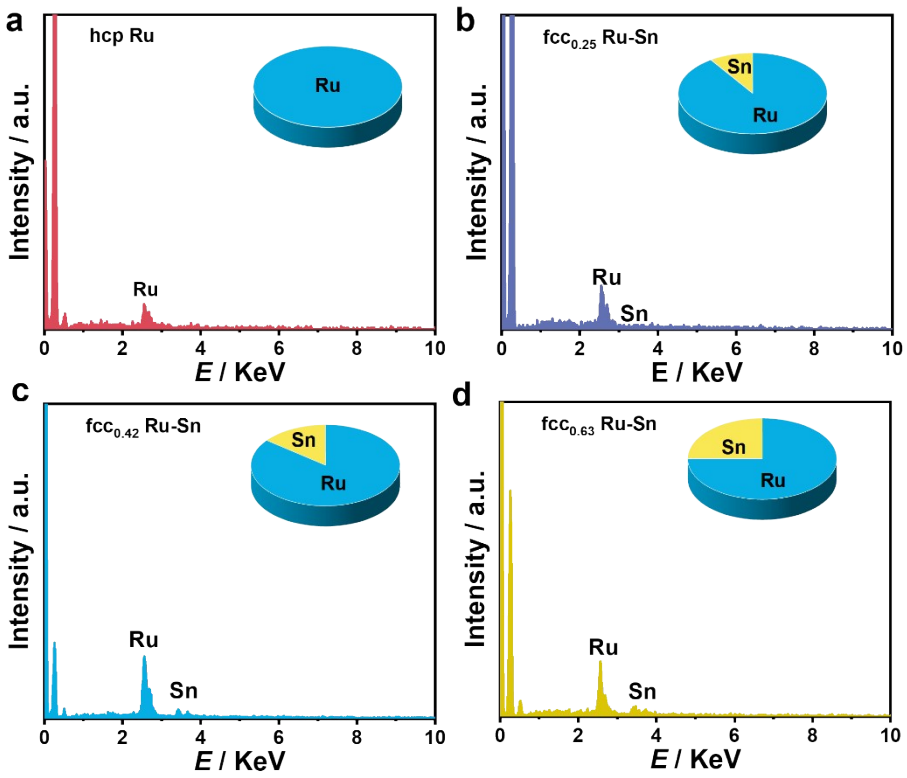

Fig. S5 EDS profiles of various samples. (a) hcp Ru, (b) $fcc_{0.25}$ Ru-Sn, (c) $fcc_{0.42}$ Ru-Sn, and (d) $fcc_{0.63}$ Ru-Sn.

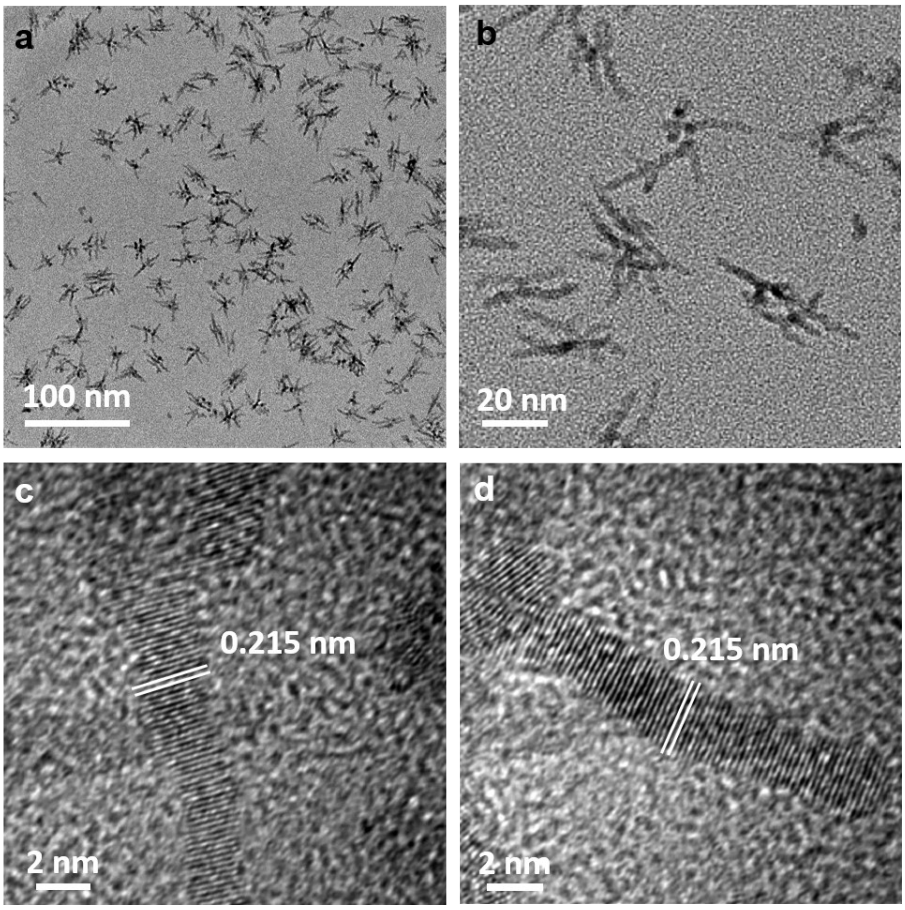

Fig. S6 (a) TEM image, (b) enlarged TEM image, (c-d) HRTEM images of hcp Ru.

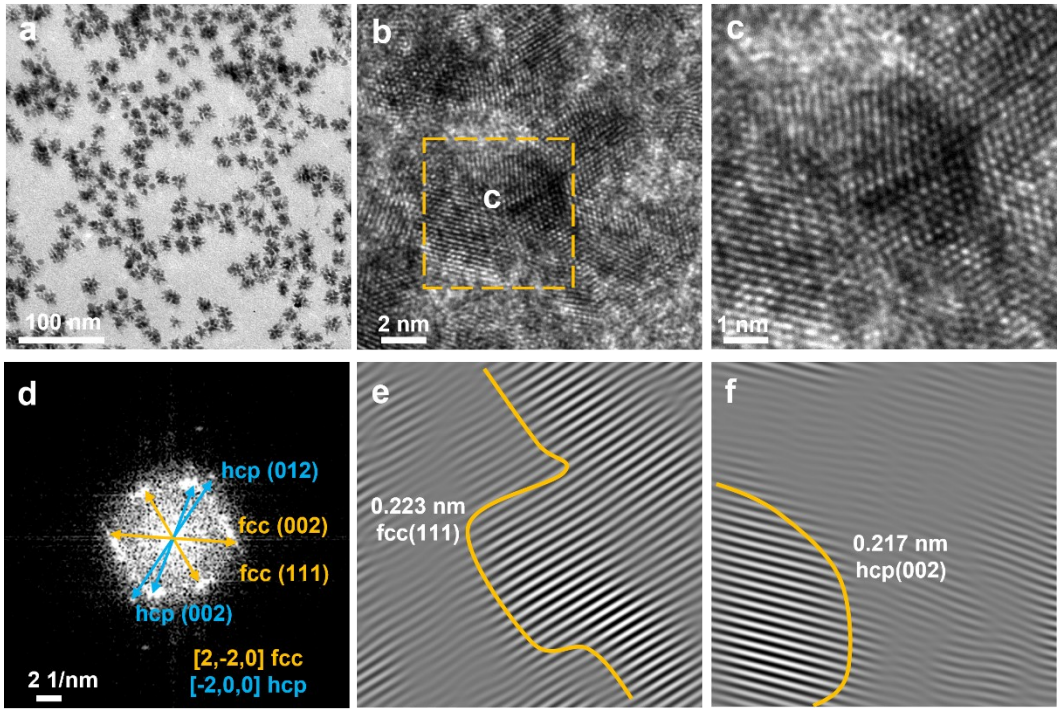

Fig. S7 (a) TEM image, (b, c) HRTEM image, (d) FFT profile, and (e, f) IFFT profiles transformed by (c) of $fcc_{0.25}$ Ru-Sn.

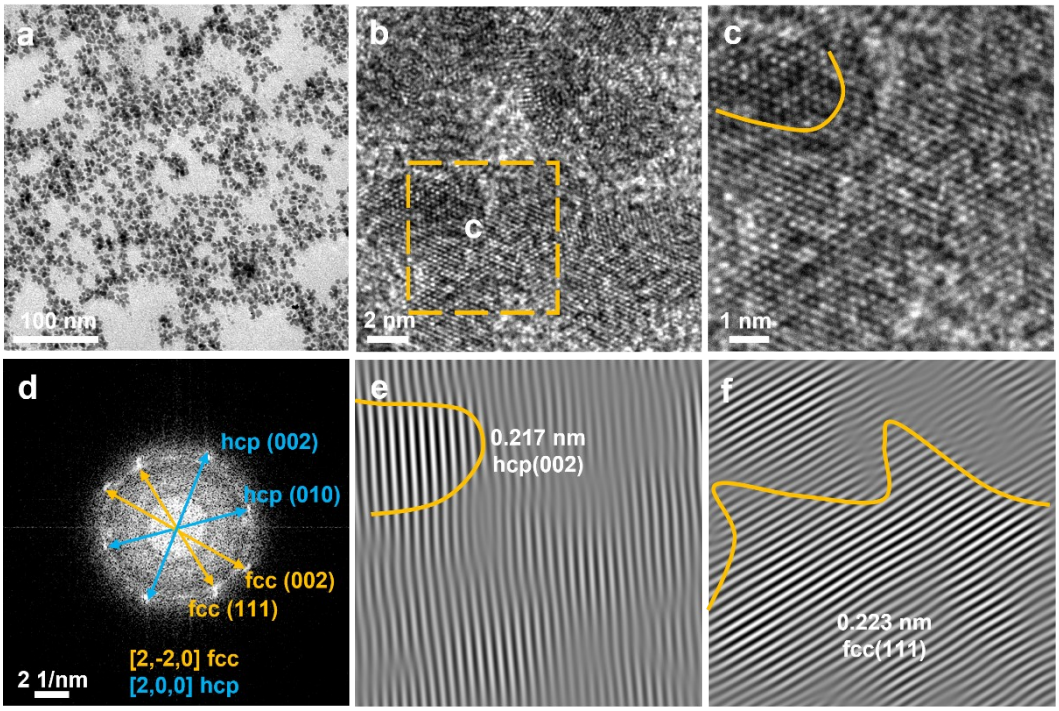

Fig. S8 (a) TEM image, (b, c) HRTEM image, (d) FFT profile, and (e, f) IFFT profiles transformed by (c) of $fcc_{0.63}$ Ru-Sn.

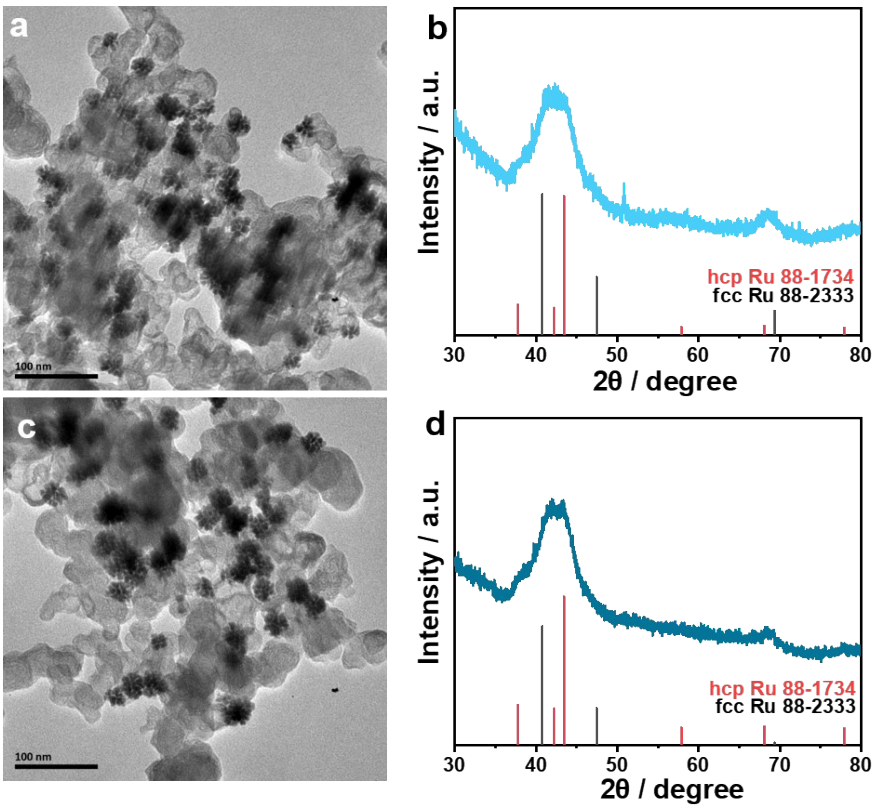

Fig. S9 (a) TEM image and (b) XRD pattern of $fcc_{0.42}$ Ru-Sn/C, (c) TEM image and (d) XRD pattern of $fcc_{0.42}$ Ru-Sn/C-250Ar.

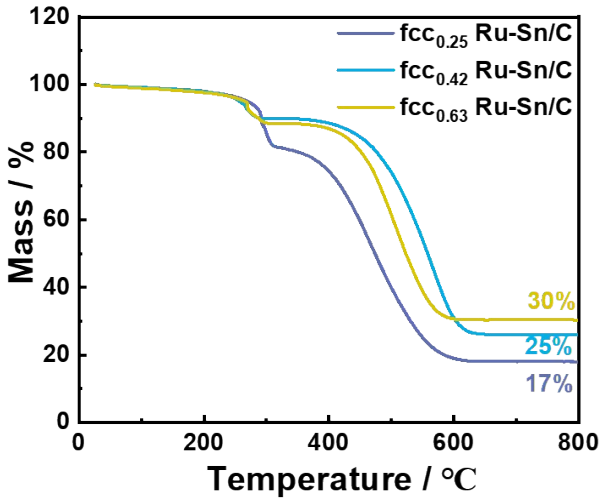

Fig. S10 TG curves of $fcc_{0.25}$ Ru-Sn/C, $fcc_{0.42}$ Ru-Sn/C and $fcc_{0.63}$ Ru-Sn/C.

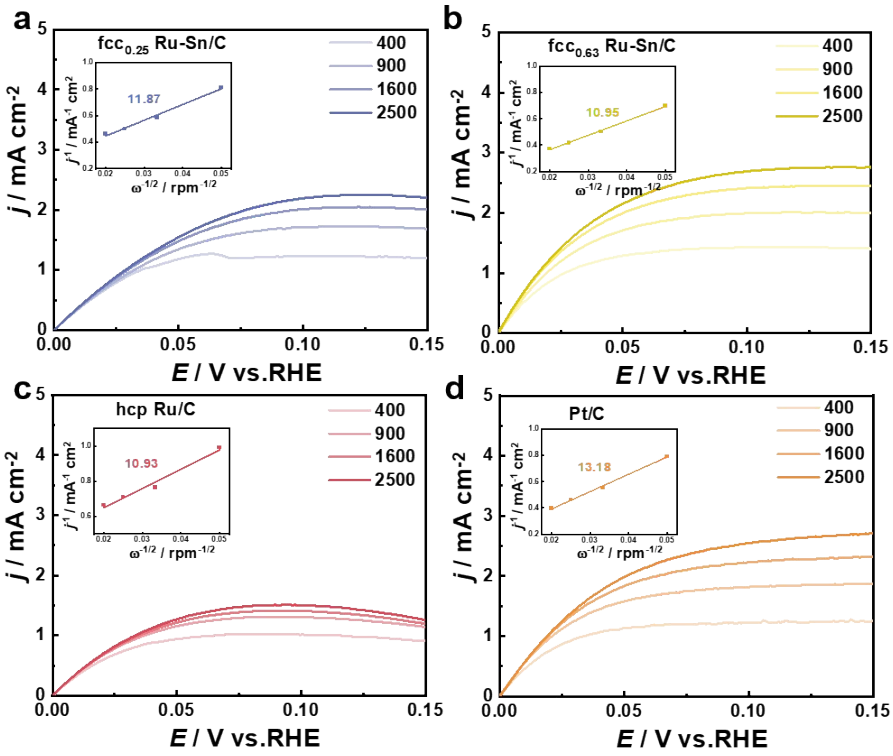

Fig. S11 HOR polarization curves of (a) $fcc_{0.25}$ Ru-Sn/C, (b) $fcc_{0.63}$ Ru-Sn/C, (c) hcp Ru/C, and (d) commercial Pt/C collected at different rotating speeds and corresponding Koutecky-Levich plots (inset) calculated at 0.1 V vs. RHE.

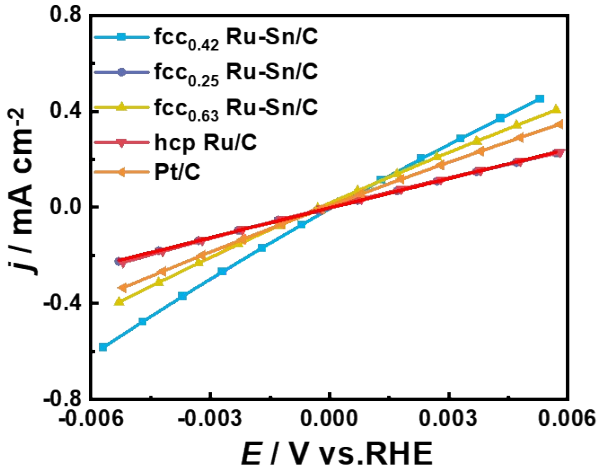

Fig. S12 Linear-fitting curves in the micro-polarization region of $fcc_{0.42}$ Ru-Sn/C, $fcc_{0.25}$ Ru-Sn/C, $fcc_{0.63}$ Ru-Sn/C, hcp Ru/C, and commercial Pt/C.

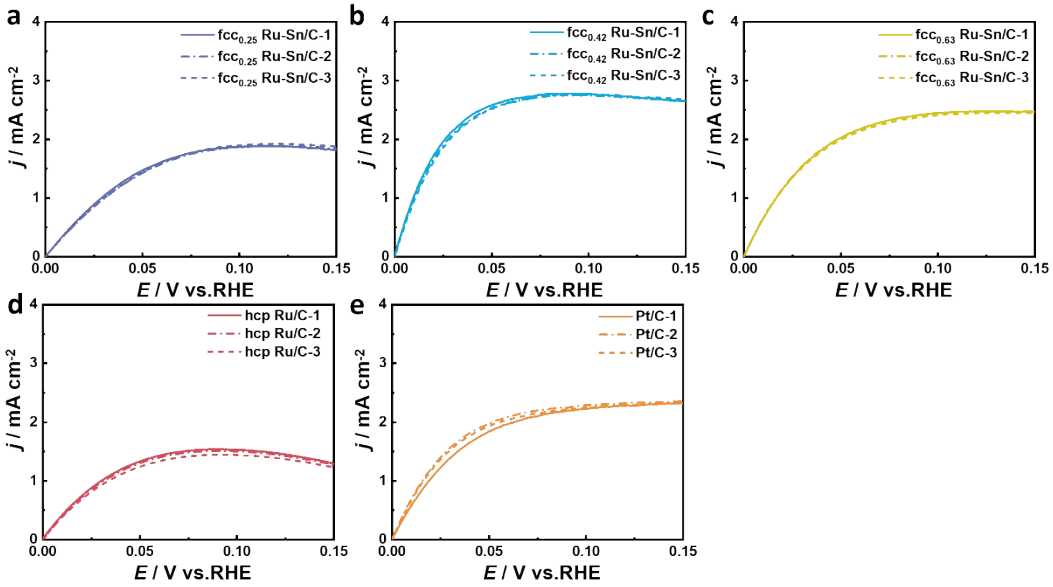

Fig. S13 (a-e) HOR polarization curves of catalysts. Each sample was tested for 3 times.

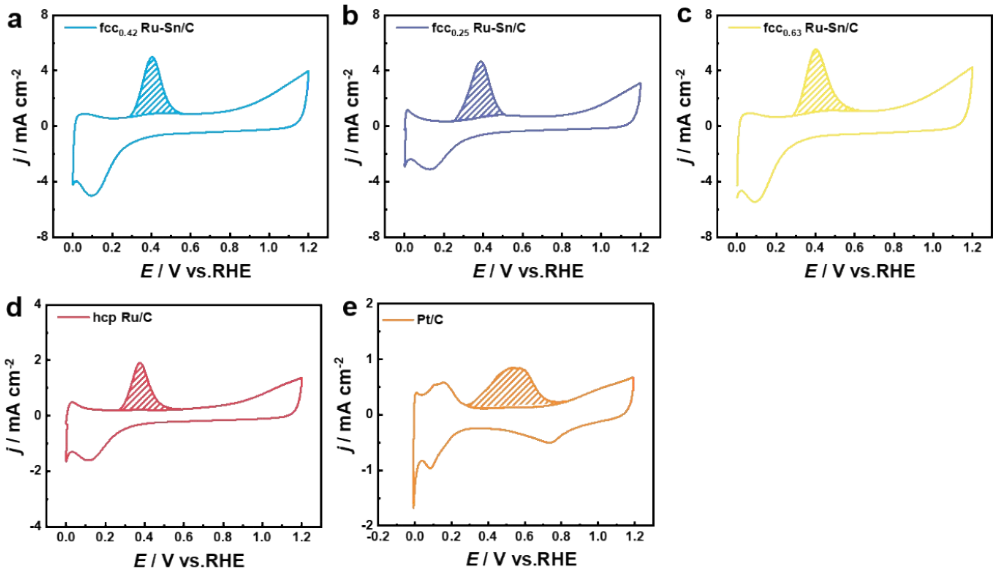

Fig. S14 (a-e) Cu stripping voltammograms of $fcc_{0.42}$ Ru-Sn/C, $fcc_{0.25}$ Ru-Sn/C, $fcc_{0.63}$ Ru-Sn/C, hcp Ru/C, and commercial Pt/C.

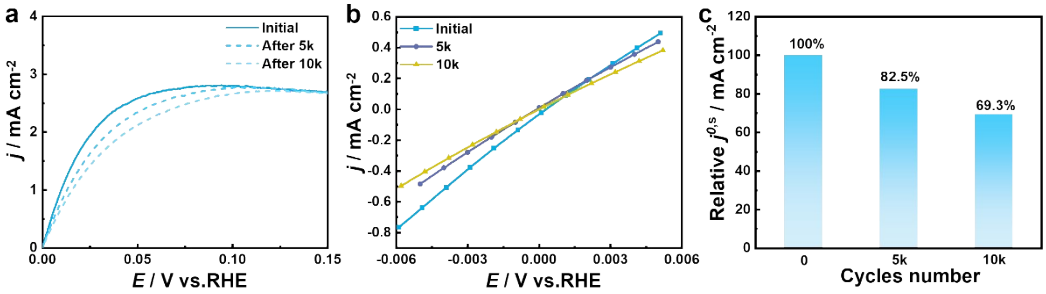

Fig. S15 (a) HOR polarization curves, (b) linear-fitting curves in the micro-polarization region, and (c) the reserved $j^{0,s}$ of $fcc_{0.42}$ Ru-Sn/C after 5 000 and 10 000 CV cycles in H_2-saturated 0.1 M KOH.

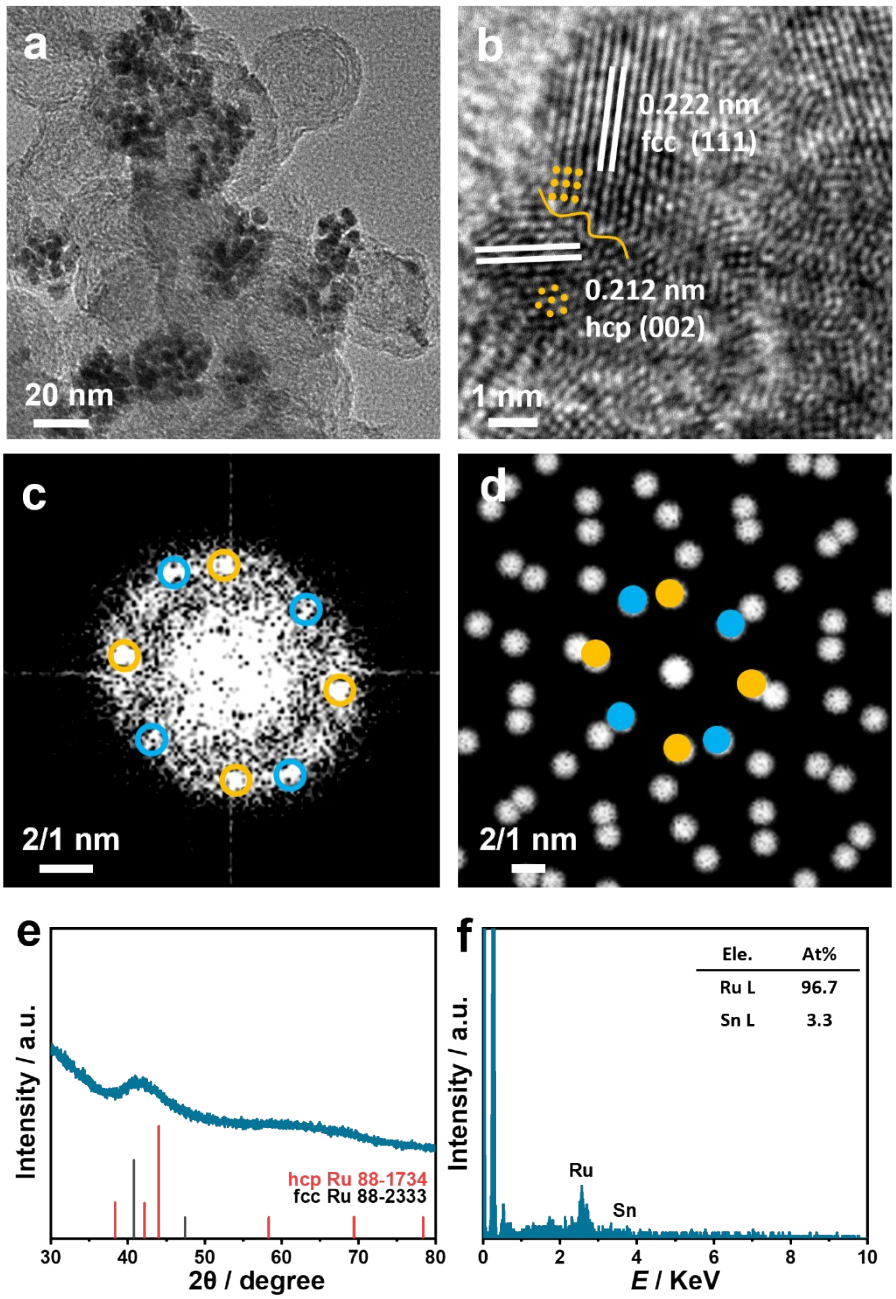

Fig. S16 (a) TEM image, (b) HRTEM image, (c, d) FFT images, (e) XRD pattern, and (f) EDS profile of $fcc_{0.42}$ Ru-Sn/C after stability test for 14 h. The blue and yellow cycles in (d) represent as hcp and fcc phase, respectively.

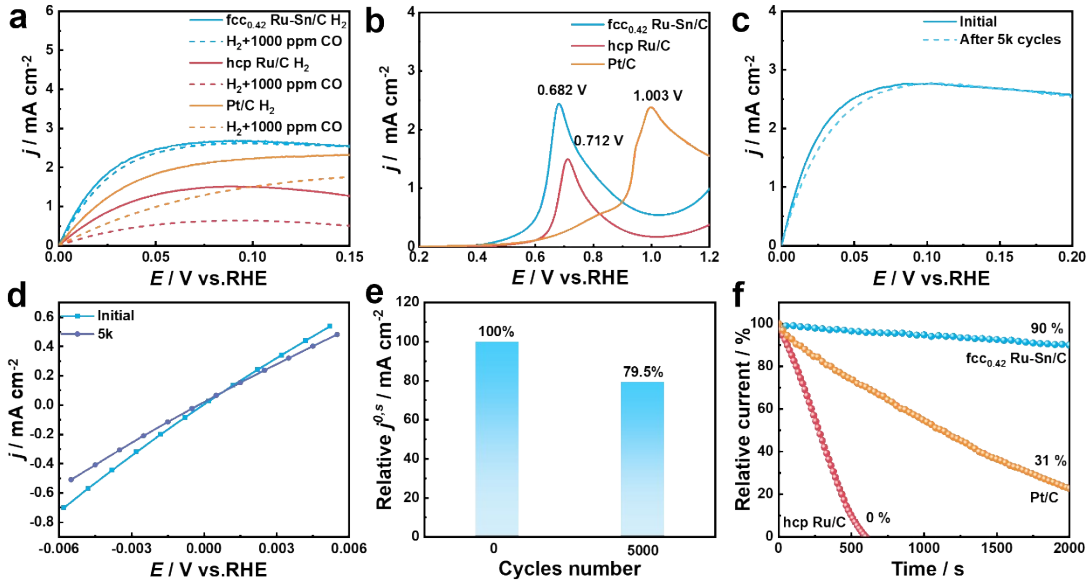

Fig. S17 (a) HOR polarization curves of hcp Ru/C, $fcc_{0.42}$ Ru-Sn/C, and Pt/C under H_2-saturated and H_2 + 1000 ppm CO-saturated 0.1 M KOH electrolyte. (b) COOR polarization curves of $fcc_{0.42}$ Ru-Sn/C, hcp Ru/C, and Pt/C. (c) HOR polarization curves, (d) linear-fitting curves in the micro-polarization region, and (e) of the reserved $j^{0,s}$ of $fcc_{0.42}$ Ru-Sn/C after 5000 CV cycles in H_2 + 1000 ppm CO-saturated 0.1 M KOH. (f) Chronoamperometric responses of catalysts at 0.1 V vs. RHE in H_2 + 1000 ppm CO-saturated 0.1 M KOH.

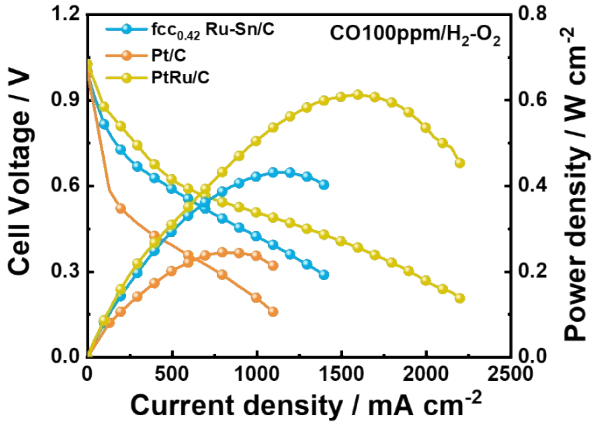

Fig. S18 Polarization and power density curves of AEMFCs with $fcc_{0.42}$ Ru-Sn/C, Pt/C or PtRu/C (0.08 mg_{Ru} cm^{-2}, 0.08 mg_{Pt} cm^{-2} or 0.08 mg_{Pt+Ru} cm^{-2}) in anode and Pt/C (0.2 mg_{Pt} cm^{-2}) in cathode. Test conditions: cell temperature at 97 °C, anode humidifier temperature at 92 °C and cathode humidifier temperature at 94 °C, back pressures were symmetric at 200 kPa, 100 ppm CO/H_2 flow rate at 1.0 L min^{-1} and O_2 flow rate at 1.0 L min^{-1}.

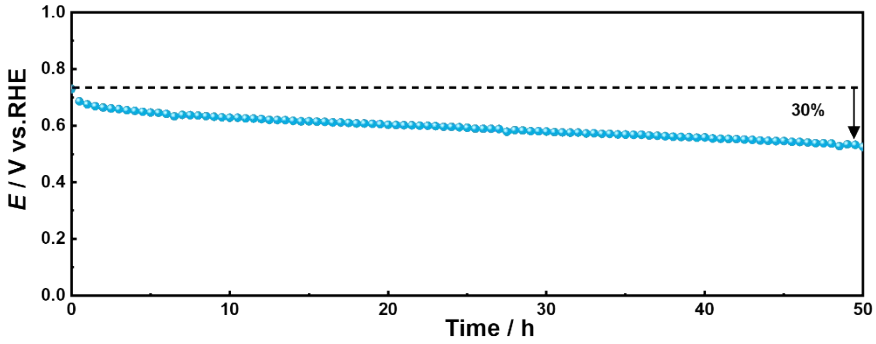

Fig. S19 H_2/O_2 AEMFCs durability test at a constant current density of 0.2 A cm^{-2} with $fcc_{0.42}$ Ru-Sn/C (0.08 mg_{Ru} cm^{-2}) as anode and Pt/C (0.2 mg_{Pt} cm^{-2}) as cathode. Test conditions: cell temperature at 80 °C, anode humidifier temperature at 79 °C and cathode humidifier temperature at 80 °C, back pressures were symmetric at 100 kPa, H_2 flow rate at 0.3 L min^{-1} and O_2 flow rate at 0.3 L min^{-1}.

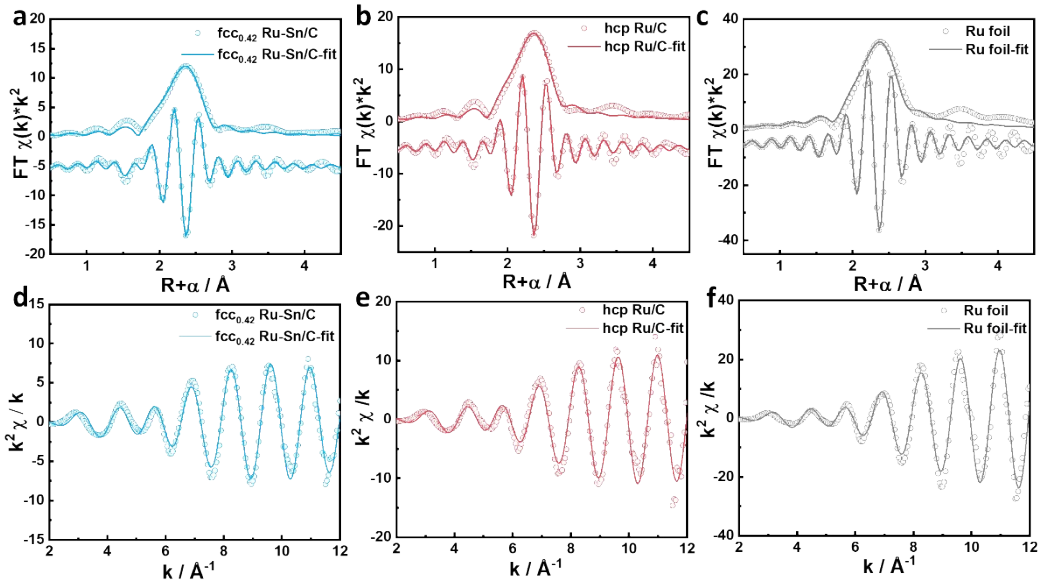

Fig. S20 The measured and fitting (a−c) R-space and (d−f) k^2-weighted k-space spectra of $fcc_{0.42}$ Ru-Sn/C, hcp Ru/C, and Ru foil at Ru K-edge.

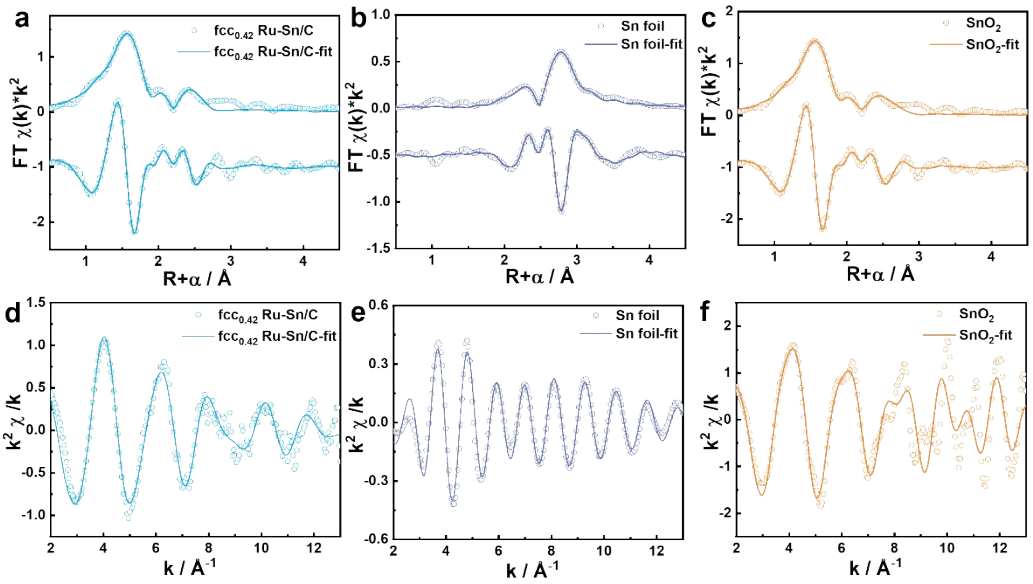

Fig. S21 The measured and fitting (a−c) R-space and (d−f) k^2-weighted k-space spectra of $fcc_{0.42}$ Ru-Sn/C, Sn foil, and SnO_2 at Sn K-edge.;

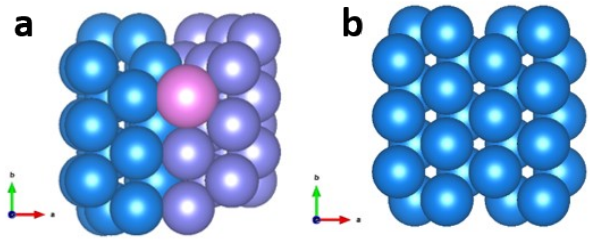

Fig. S22 The optimized structures of (a) $fcc_{0.42}$ Ru-Sn and (b) hcp Ru. hcp Ru atom: blue, fcc Ru atom: purple, and Sn atom: pink.

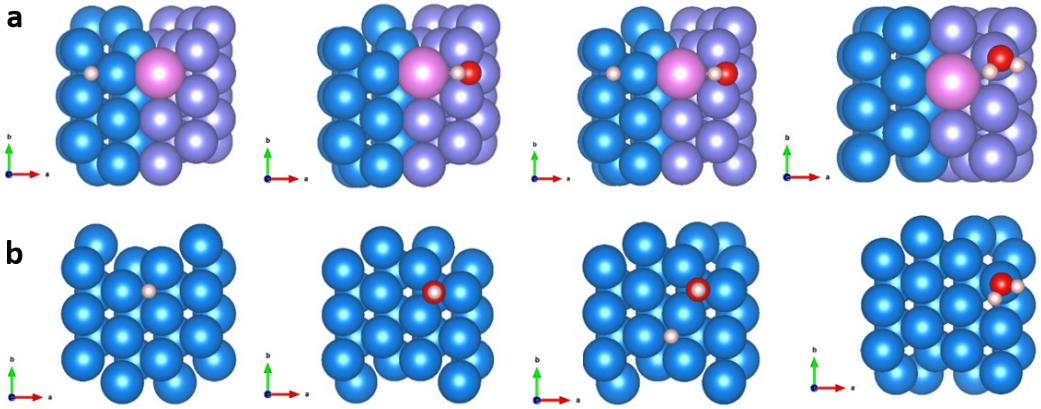

Fig. S23 The optimized adsorption structures of (a) $fcc_{0.42}$ Ru-Sn and (b) hcp Ru. hcp Ru atom: blue, fcc Ru atom: purple, Sn atom: pink, H atom: white, and O atom: red.

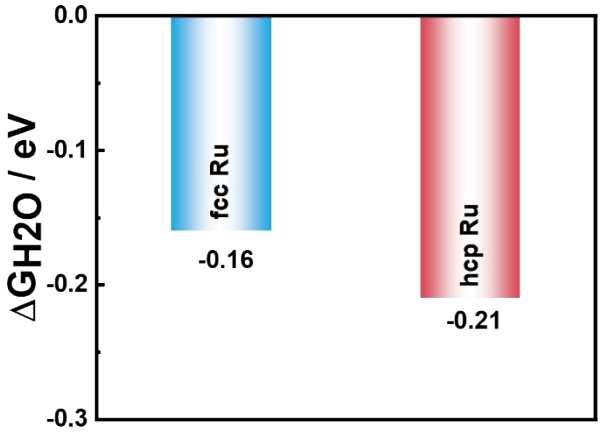

Fig. S24 H_2O adsorption Gibbs free energy of fcc and hcp catalytic sites on $fcc_{0.42}$ Ru-Sn catalyst.

Table S1 Structural parameters for Rietveld refinement.

	element	occupancy	x	y	z	uiso	R_{wp}	R_p	χ^2
hcp Ru							2.23%	1.69	1.735
hcp phase	Ru	1	0.3333	0.6667	0.25	0.01105			
$fcc_{0.25}$ Ru-Sn							1.85%	1.47	1.101
fcc phase	Ru1	0.948	0	0	0	0.01232			
	Sn	0.052	0	0	0	0.00937			
hcp phase	Ru	0.984	0.3333	0.6667	0.25	0.0119			
	Sn	0.016	0.3333	0.6667	0.25	0.01594			
$fcc_{0.42}$ Ru-Sn							2.75%	2.12	1.165
fcc phase	Ru1	0.919	0	0	0	0.01217			
	Sn	0.081	0	0	0	0.01219			
hcp phase	Ru	0.993	0.3333	0.6667	0.25	0.01261			
	Sn	0.007	0.3333	0.6667	0.25	0.00837			
$fcc_{0.63}$ Ru-Sn							1.70%	1.32	1.093
fcc phase	Ru1	0.782	0	0	0	0.00719			
	Sn	0.218	0	0	0	0.00455			
hcp phase	Ru	0.993	0.3333	0.6667	0.25	0.01261			
	Sn	0.007	0.3333	0.6667	0.25	0.00837			

Table S2 The mass activity, exchange current, specific activity, and exchange current density.

Samples	$\mathbf{j^{k,\,m}}$	$\mathbf{i^{0}}$	$\mathbf{j^{0,s}}$	$\mathbf{j^{0\text{-}ML}}$
$fcc_{0.42}$ Ru-Sn/C	4.9	1.7	6.7	2.1
$fcc_{0.25}$ Ru-Sn/C	0.7	0.3	0.9	1.0
$fcc_{0.63}$ Ru-Sn/C	1.7	0.6	2.2	1.8
hcp Ru/C	0.5	0.3	0.9	1.1
Pt/C	1.3	0.4	1.9	1.6

Table S3 Comparison between $fcc_{0.42}$ Ru-Sn/C and other reported catalysts for alkaline HOR.

Catalysts	Electrolyte	Mass activity / A mg^{-1}	Refs
$fcc_{0.42}$ Ru-Sn/C	**0.1 M KOH**	**4.9**	**This work**
$Ru_{0.95}Co_{0.05}$/C	0.1 M KOH	0.15	Ref 8
Mo-Ru NSAs	0.1 M KOH	2.45	Ref 9
Cu_2O@Rufcc/C	0.1 M KOH	0.396	Ref 11
Ru_7Sn_3	0.1 M KOH	0.658	Ref 25
RhSn	0.1 M KOH	0.246	Ref 26
Sn-Ru/C	0.1 M KOH	1.79	Ref 27
$Pb_{1.04}$-$Ru_{92}Cu_8$/C	0.1 M KOH	1.10	Ref 28
$RuFe_{0.1}$	0.1 M KOH	0.23	Ref 29
RuNi	0.1 M KOH	4.34	Ref 30
P-RuC	0.1 M KOH	0.9	Ref 31
Ir_1Ru_3 NWs	0.1 M KOH	3.35	Ref 32
Ru/C-H_2O/CH_3CH_2OH	0.1 M KOH	0.037	Ref 33
Ru-Ru_2P/C	0.1 M KOH	1.265	Ref 34
Ir@Pd	0.1 M KOH	0.025	Ref 35

Table S4 Comparison performance of AEMFCs assembled with $fcc_{0.42}$ Ru-Sn/C and other reported catalysts.

Anode catalysts	**Cathode catalysts**	**Backpressure Kpa**	**T_{cell} °C**	**PPD W cm^{-2}**	**PPD W mg_{PGM}^{-1}**	**Refs.**
$fcc_{0.42}$ RuSn/C 0.08 mg cm^{-2}	**Pt/C 0.2 mg cm^{-2}**	**200**	**97**	**0.997**	**12.46**	**This work**
Ru/Meso C 0.1 mg cm^{-2}	Pt/C 0.45 mg cm^{-2}	200	80	1.02	10.2	*J Power Sources*, 2020, **461**, 228147
IrRu NWs/C 0.1 mg cm^{-2}	Pt/C 0.3 mg cm^{-2}	100	60	0.485	4.85	*J. Mater. Chem. A,* 2018, **6**, 20374−20382
Ru_7Ni_3 0.2 mg cm^{-2}	Pt/C 0.4 mg cm^{-2}	250	97	2.03	10.15	*Nat. Commun.*, 2020, **11**, 5651
RuPdIr/C 0.2 mg cm^{-2}	Pd/C 0.1 mg cm^{-2}	200	80	0.820	4.1	*Chem. Commun.*, 2020, **56**, 5669−5672
Ru/VOC 0.34 mg cm^{-2}	Pt/C 0.4 mg cm^{-2}	100	92	1.19	3.51	*J. Am. Chem. Soc.,* 2023, **145**, 27867−27876
Ru-Fe/C 0.4 mg cm^{-2}	Pt/C 0.4 mg cm^{-2}	200	80	1.20	3.0	*Small*, 2022, **18**, 2202404
RuCr-2 0.4 mg cm^{-2}	Pt/C 0.4 mg cm^{-2}	200	80	1.04	2.6	*Chin. J. Chem.*, 2022, **40**, 2495−2501
B-Ru/C 0.42 mg cm^{-2}	Pt/C 0.48 mg cm^{-2}	250	95.5	1.37	3.26	*Adv. Mater.* 2024, **36**, 2304496
Ru/C 0.5 mg cm^{-2}	Pt/C 0.5 mg cm^{-2}	–	50	0.25	0.5	*J Power Sources*, 2013, **225**, 311−315

Table S5 Fitting results of EXAFS data at Ru *K*-edge.

Samples[a]	**Path**	**CN**[b]	**R/Å**[c]	**$\sigma^2/10^{-3}$Å^2**[d]	**ΔE_0**[e]	**R-factor**
Ru foil	Ru−Ru	12	2.68 ± 0.002	1.79 ± 1.68	−1.8 ± 2.5	0.02
$fcc_{0.42}$ Ru-Sn/C	Ru−Ru	4.1 ± 0.9	2.67 ± 0.025	5.14 ± 1.24	−4.8 ± 1.5	0.01
hcp Ru/C	Ru−Ru	4.9 ± 0.9	2.67 ± 0.025	3.63 ± 1.27	−3.4 ± 1.6	0.01

[a] s^0 was fixed to 0.9, data range 3.0 < k (Å) <12.2 and 1.8 < R (Å) < 3.2, [b] coordination number, [c] bonding distance; [d] the Debye-Waller factor, [e] inner potential shift.

Table S6 Fitting results of EXAFS spectra at Sn *K*-edge.

Samples[a]	Path	CN[b]	R/Å[c]	$\sigma^2/10^{-3}$Å^{2}[d]	ΔE_0[e]	R-factor
$fcc_{0.42}$ Ru-Sn/C	Sn−O	5.8 ± 0.5	2.04 ± 0.02	4.5 ± 1.1	3.2 ± 1.1	0.02
	Sn−Ru	1.8 ± 0.5	2.78 ± 0.04	8.0 ± 0.0		
Sn foil	Sn−Sn	4	3.00 ± 0.02	9.38 ± 1.38	−3.5± 0.7	0.02
	Sn−Sn	2	3.17 ± 0.02	9.81 ± 4.95		
SnO_2	Sn−O	6	2.05 ± 0.01	2.54 ± 0.59	−5.6 ± 0.5	0.01
	Sn−Sn	2	3.20 ± 0.01	1.53 ± 2.09		

[a] s^0 was fixed to 0.8, data range 2.8 < k (Å) < 13 and 1 < R (Å) < 2.8, [b] coordination number, [c] bonding distance; [d] the Debye-Waller factor, [e] inner potential shift.

References:

1 N. Chen, H. H. Wang, S. P. Kim, H. M. Kim, W. H. Lee, C. Hu, J. Y. Bae, E. S. Sim, Y. C. Chung, J. H. Jang, S. J. Yoo, Y. Zhuang and Y. M. Lee, *Nat Commun*, 2021, **12**, 2367.

2 G. Kresse, J. Furthmuller, *Phys. Rev. B* 1996, **54**, 11169-11186.

3 P. E. Blochl, *Phys. Rev. B* 1994, **50**, 17953−17979.

4 J. P. Perdew, K. Burke, M. Ernzerhof, *Phys. Rev. Lett.* 1996, **77**, 3865−3868.

5 S. Grimme, J. Antony, S. Ehrlich, H. Krieg, *J. Chem. Phys.* 2010, **132**, 154104.

6 V. Wang, N. Xu, J. C. Liu, G. Tang, W. T. Geng, Comput. *Phys. Commun.* 2021, **267**, 108033.